Journal of Organometallic Chemistry 934 (2021) 121659

Contents lists available at ScienceDirect

Journal of Organometallic Chemistry

journal homepage: www.elsevier.com/locate/jorganchem

Ionic Ruthenium and Iron Based Complexes Bearing Silver Containing Anions as a Potent New Class of Anticancer Agents ☆

Amal Benamrane [a], Brian Herry [a], Veacheslav Vieru [a], Suparna Chakraborty [b], Supratim Biswas [b], Sharon Prince [b,*], Christoph Marschner [c], Burgert Blom [a,*]

[a] Maastricht Science Programme, Faculty of Science and Engineering, Maastricht University, Paul-Henri Spaaklaan 1, 6229 EN Maastricht, The Netherlands
[b] University of Cape Town, Department of Human Biology, Observatory 7935, Cape Town, South Africa
[c] Institut für Anorganische Chemie, Technische Universität Graz, Stremayrgasse 9, A-8010 Graz, Austria

ARTICLE INFO

Article history:
Received 25 November 2020
Revised 16 December 2020
Accepted 16 December 2020
Available online 19 December 2020

Keywords:
Anticancer agents
Ruthenium cation
Silver anion
Breast cancer
in vitro testing

ABSTRACT

A series of salt complexes of the type $[RuCl(\eta^6\text{-arene})(\kappa^2\text{-dppm})]^+[AgCl(hfac)(PMe_3)]^-$(arene = benzene (**1a**) or *p*-cymene (**1b**), hfac = hexafluoroacetylacetato, dppm = 1,1-bis(diphenylphosphino)methane) have been prepared in a facile route by reaction of $[RuCl_2(\eta^6\text{-arene})(\kappa^1\text{-dppm})]$ with $[Ag(hfac)(PMe_3)]$. The iron complex: $[CpFe(CO)(\kappa^2\text{-dppm})]^+$ $[AgI(hfac)(PMe_3)]^-$ (**4**) (Cp = η^5-C_5H_5) was also isolated in an analogous fashion by reacting the known complex $[CpFeI(CO)(\kappa^1\text{-dppm})]$ with $[Ag(hfac)(PMe_3)]$. The complexes were fully characterised by spectroscopic means including multinuclear NMR spectroscopy, IR, ESI-MS and UV-Vis. In all cases broad signals are observed in the $^{31}P\{^1H\}$ NMR spectra corresponding to the P atom in the anion $[AgX(hfac)(PMe_3)]^-$ (X = Cl or I) which suggests fluxional behaviour. Confirming this picture, the single crystal X-ray diffraction analysis of $[CpFe(CO)(\kappa^2\text{-dppm})]^+[hfac]^-$ (**4-D**) is presented, obtained as a decomposition product of compound **4** corresponding with the loss of "$AgI(PMe_3)$". The nature of the elusive anion $[AgX(hfac)(PMe_3)]^-$ was investigated by DFT methods (BP86 functional, the ma-def2-SVP basis set for all atoms) showing a weak interaction between the oxygen atoms of the $hfac^-$ moiety and the Ag centre. Calculated IR spectra were compared to those obtained experimentally and show an excellent agreement, confirming this picture. The *in vitro* cytotoxicity on two breast cancer cell-lines (MCF-7 and MDA-MB-231) of all compounds is reported and compared to cisplatin as positive control. The tetrafluoroborate complexes: type $[RuCl(\eta^6\text{-arene})(\kappa^2\text{-dppm})]^+BF_4^-$ (arene = benzene (**2a**) or p-cymene (**2b**)) were also prepared and tested in order to elucidate the effect of the silver anion on cytotoxicity and selectivity in **1a** and **1b**. Moreover, the complex $[CpFe(CO)(\kappa^2\text{-dppm})]^+BF_4^-$ (**3**) was also prepared for comparison to **4**, bearing the silver anion. In general, all complexes exhibit remarkable cytotoxicity and selectivity profiles on both cell-lines, and out-perform cisplatin. The presence of silver in the anion (in compounds **1a, 1b** and **4**) on average enhance their cytotoxicity compared to their corresponding BF_4 analogues. The most active and selective in the entire series is compound **4**, which demonstrates that these compounds represent high potential in anticancer applications. Moreover, compounds **4** and **1a** inhibited the long-term survival and migration of oestrogen receptor positive (MCF-7) and triple negative (MDA-MB-231) breast cancer cell lines tested respectively. Additionally, compounds **4** and **1a** induced morphological and molecular characteristics of apoptosis in MCF-7 and MDA-MB-231 breast cancer cells respectively.

1. Introduction

Metal-based drugs are fundamental in treatment protocols for various types of cancer [1a,b]. The highly selective platinum-based drugs, in particular the seminal drug cisplatin [2a,b]: *cis*-$[PtCl_2(NH_3)_2]$ (Fig. 1a) have made a remarkable impact in cancer therapy. Platinum based drugs are known for targeting the DNA of tumour cells, preventing cell replication and tumour development [1b]. Currently, several other platinum based agents are also effec-

☆ Dedicated to Prof. Paul Dyson and his many contributions to the field of organometallic cancer agents

* Corresponding authors.
E-mail addresses: sharon.prince@uct.ac.za (S. Prince), burgert.blom@maastrichtuniversity.nl (B. Blom).

https://doi.org/10.1016/j.jorganchem.2020.121659
0022-328X/

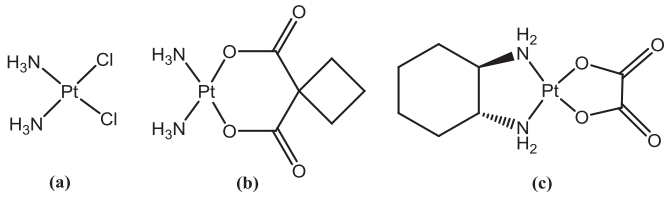

Fig. 1. cisplatin (a) carboplatin (b) oxaliplatin (c).

tively being used, such as carboplatin [3c-d] or oxaliplatin [4a-c] (Fig. 1 b, and c), which show lower toxic side effects than cisplatin [4c, 5a,b]. Unfortunately, the use of platinum has severe drawbacks in terms of toxicity, side effects and chemoresistance [6a,b]. This has precipitated interest in the development of new alternative cancer agents bearing other transition metals as active centres.

Transition metals such as titanium [7a,b], iron [8a-c], ruthenium [9a-d], silver [10a-f] are known for their rich coordination chemistry, which offers opportunities to synthesize compounds, which may exhibit anticancer activity. Iron has been researched thoroughly because of its high abundance, low cost, and utmost importance in several proteins and enzymes and metabolic processes [8c]. Due to biocompatibility, iron represents an element which is ideal in anticancer metallodrugs. Since the discovery of the chemotherapeutic properties of ferrocenium salts in 1984 [8a], many developments in iron based cytotoxic agents have been accomplished [8b-d]. Reports on piano stool complexes bearing η^5-C_5H_5 ligands (Cp), as the ones shown in Fig. 2 have also appeared; for example, cationic Fe-Cp species with different phosphane co-ligands have proven to be highly cytotoxic, causing cell death by apoptosis in human cancer cells [8d].

Another metal that has gained considerable interest in recent years is ruthenium. The Ru-based metallodrugs KP1019 [9c] and NAMI-A [9a] (Fig. 3), have been shown to be promising agents. Encouraging research has also been reported on organometallic Ru-arene complexes containing phosphane ligands. Examples of these complexes that underwent *in vivo* and *in vitro* testing are RAPTA-B [9b] [Ru(η^6-C_6H_6)(pta)Cl_2] and RAPTA-C [9b,e] [Ru(η^6-*p*-cymene)(pta)Cl_2] (pta =1,3,5-triaza-7-phosphaadamantane) (Fig. 3). The results show that these complexes reduce the growth of lung metastases in CBA (inbred strain) mice [9b], as well as inhibiting the growth of tumours in human ovarian and colorectal carcinomas transplanted onto chickens [9e]. Additionally, the results indicate that ruthenium is rapidly removed from organs and the bloodstream [9b,e]. However, much is still unknown in terms of the mechanism of action of ruthenium based drugs [9b,d].

A further novel and promising strategy in the synthesis of metal complexes as chemotherapeutic agents, is the incorporation of silver. Specifically, silver phosphane complexes were reported to be cytotoxic against certain types of cancer [10a-f]. A broad range of different silver phosphane complexes have been studied (Fig. 4) in order to evaluate their anticancer activity towards a malignant SNO (South African esophageal carcinoma) cell line. The outcome was compelling since the majority of the tested complexes were found to be highly toxic towards the cancer cells and significantly less toxic towards healthy cells [10e]. This research among others opened the way to create many new potential anticancer agents containing silver. In fact, even more recent studies have shown that silver(I) thiocyanate monophosphane complexes are selective towards apoptosis of breast cancer cells [10c] and esophageal cancer cell lines [10b]. This led to the discovery of the so called “silver bullet” in patented work by Engelbrecht et al. in 2018 [10f]. They have shown that a silver(I) thiocyanate 4-methoxyphenyl phosphine complex, effectively induces cell death in esophageal cancer cells, but displays low cytotoxicity towards healthy skin and kidney cell lines [10f].

The incorporation of several metal atoms into a well-defined molecular structure, has also gained considerable attention. Bimetallic or even multimetallic anticancer drugs have been explored, in order to exploit the cytotoxic properties of each metal and overcome resistance with a view of potential synergic effects. Examples of such bimetallic systems are shown in Fig. 5. Massai et al. [11] have reported the seminal synthesis of ruthenium(II)-gold(II) complexes and tested these for cytotoxic activity (Fig. 5a). The results indicated more favourable properties in terms of both selectivity and anticancer activity. This strongly supports the idea that heterometallic systems may represent improved chemotherapeutic agents, compared to their mononuclear systems [11]. Another notable example is the work by Wenzel et al. [12], in which heterodinuclear Pt-Ag complexes were tested and compared to their mononuclear Au(I) counterparts. The results were optimistic since some of the compounds were able to overcome possible chemoresistance and showed anticancer properties. However, it was found that the cytotoxicity for the bimetallic derivatives has not been improved drastically in comparison to their mononuclear complexes, hence more research is needed [12].

Due to the promising cytotoxicity of ruthenium arene complexes and the growing success of bimetallic systems, we recently reported the synthesis of novel Ru,Ru homobimetallic (Fig. 6) and Fe,Ru heterobimetallic systems as potential anticancer agents [13]. Both Ru,Ru and Fe,Ru complexes were tested on A2780, A2780cisR and HEK293 cell lines and it was shown that the Fe,Ru systems outperform cisplatin, and show a moderate degree of cancer-cell selectivity, while the dinuclear Ru systems performed less well across all cell-lines. The potential of incorporation of Fe into the molecular architecture of the complexes was hence uncovered.

As part of our ongoing research programme into the development of heterobimetallic systems that may exhibit enhanced cytotoxic profiles, we concentrated on the preparation of Ru,Ag and Fe,Ag complexes, reasoning that combining these two elements into one molecule may enhance cytotoxic activity (see above).

In this report, the novel salt complexes: [RuCl(η^6-arene)(κ^2-dppm)]$^+$[AgCl(hfac)PMe_3]$^-$ (arene = C_6H_6 (**1a**) and arene = *p*-cymene (**1b**), dppm = 1,1-bis(diphenylphosphino)methane) as well as a related iron complex [Fe(CO)(η^5-C_5H_5)(κ^2-dppm)]$^+$[AgI(hfac)PMe_3]$^-$ (**4**) have been prepared and fully characterised by spectroscopic methods and subjected to *in vitro* cytotoxicity studies on the breast cancer cell-lines MCF-7 and MDA-MB-231, showing remarkable cytotoxicity and selectivity profiles. These are compared with the corresponding BF_4^- salts to delineate the effect of the silver anions on cytotoxicity. In all cases, the complexes exhibit increased cytotoxicity and selectivity compared to cisplatin. Other biological studies (clonogenic assays, scratch mobility studies, apoptosis studies) are also reported here which highlight these complexes show particular promise as potential anti-cancer agents.

2. Results and Discussion

The reaction between the known complex [$RuCl_2$(η^6-arene)(κ^1-dppm)] [13] (arene = benzene and *p*-cymene) and [Ag(hfac)PMe_3] resulted in the formation of an ionic species (**1a** and **1b**) (Scheme 1). It was expected the PMe_3 ligand would be liberated *via* a nucleophilic attack of the pendant P atom of the dppm at the silver centre, forming the neutral heterobimetallic complex [$RuCl_2$(η^6-arene)(μ-dppm)Ag(hfac)]. However, halide abstraction from the Ru centre and the formation of salt compounds: [RuCl(η^6-arene)(κ^2-dppm)]$^+$[AgCl(hfac)(PMe_3)]$^-$ (**1a**: arene = benzene, **1b**: arene = *p*-cymene) proceeded instead (Scheme 1). From

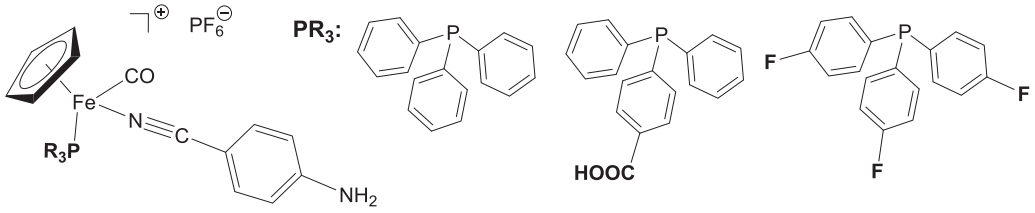

Fig. 2. Iron-Cp complexes [8d] tested for cytotoxic activity.

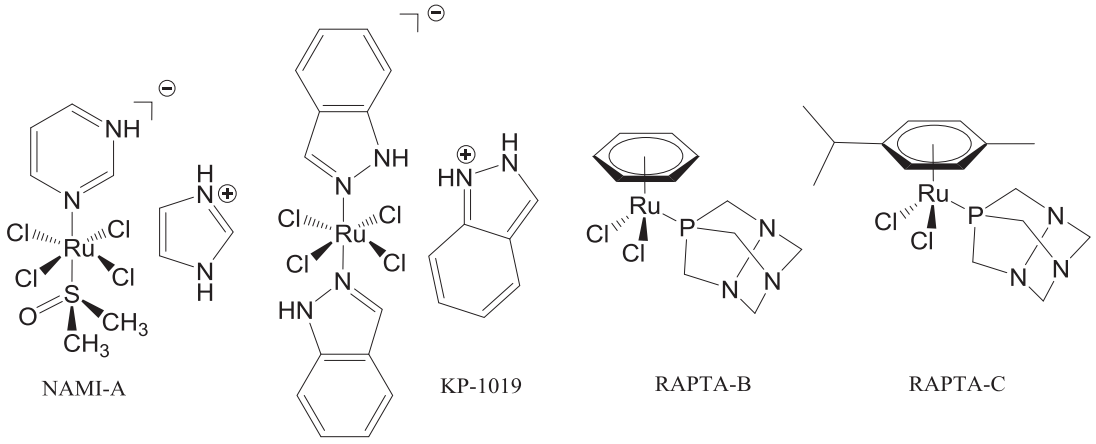

Fig. 3. A selection of metallodrugs based on ruthenium.

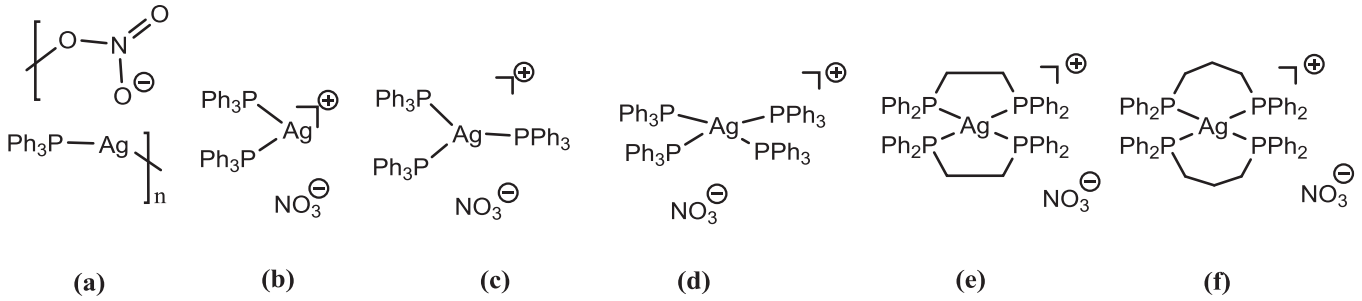

Fig. 4. Different silver phosphane complexes tested for cytotoxic activity [10e].

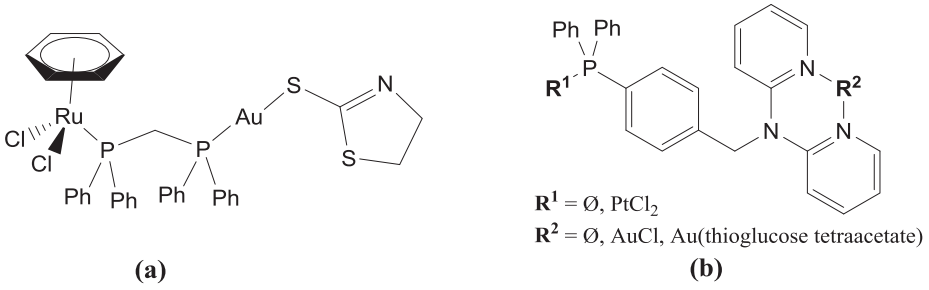

Fig. 5. Multiple examples of heterobimetallic systems (a) Ru-Au [11], (B) Pt-Au [12]

the heteronuclear NMR spectra, it became evident that the cation is $[RuCl(\eta^6\text{-arene})(\kappa^2\text{-dppm})]^+$, in which the dppm is connected in a bidentate fashion to the ruthenium centre. The $^{31}P\{^1H\}$ NMR spectrum of **1a** shows a sharp singlet at $\delta = 2.46$ confirming equivalence of the coordinated P atoms. A broad signal at δ = -36.7 corresponds to the PMe_3 attached to the silver complex anion and the broadness of the signal suggests a dynamic process in solution, involving the PMe_3-group. The obtained ^1H NMR spectrum of **1b** is consistent with literature data [14b,c] of the cation in $[RuCl(\eta^6\text{-}p\text{-cymene})(\kappa^2\text{-dppm})]BF_4$ (**2b**). As with **1a** its ^{31}P NMR spectra also reveal two signals, the high-field shifted signal being broadened by a dynamic process, and a sharp low-field signal corresponding to the Ru cation. The two analogues **2a** and **2b**, with BF_4^- as the anion, were also synthesised as a reference to test the effect of the different anion in terms of cytotoxicity. Numerous attempts at growing crystals of **1a** and **1b** were unsuccessful and typically resulted in decomposition over several weeks and concomitant deposition to a white/grey precipitate.

Additionally, the ESI(+) of **1a** and **1b** confirmed the presence of the chelated ruthenium cation, in accord with the NMR data, and

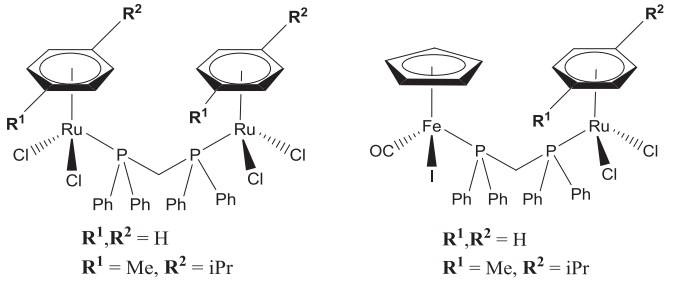

Fig. 6. Homobimetallic Ru-Ru and Heterobimetallic Fe-Ru systems previously reported.

showed the cation as the base peak (100 % abundance) with very little other fragmentation visible in the spectrum (see SI). However in both **1a** and **1b**, the ESI(-) exhibited a high intensity signal corresponding to the *hfac*-backbone: $hfac^-$, and no signal corresponding to $[AgCl(hfac)(PMe_3)]^-$ was detected, even at very low intensity. This may suggest that the "$AgCl(PMe_3)$" moiety is only weakly bound to the $hfac^-$ and undergoes fragmentation in the mass spectrometer, even utilising a soft ionization technique (ESI). In fact, the exact nature of the anion is a weakly bound adduct between $AgCl(PMe_3)$ and the negatively charged hfac: $[AgCl(PMe_3)\cdot hfac]^-$as elucidated by detailed DFT investigations (see below).

Broadening the scope of this reaction and exploring its generality, we attempted the analogous reaction of the iron precursor: $[CpFeI(CO)(\kappa^1\text{-dppm})]$ with $[Ag(hfac)(PMe_3)]$. Strikingly, the reaction proceeds in the same fashion (Scheme 2) and resulted in the isolation of the salt complex: $[CpFe(CO)(\kappa^2\text{-dppm})]^+[AgI(hfac)(PMe_3)]^-$ (**4**) in good yields as a brown solid as a hexane solvate. The NMR spectra are akin to that of **1a** and **1b** where for example in the $^{31}P\{^1H\}$ NMR spectrum two sets of resonance signals are observed, corresponding to the cation (sharp singlet) which is low-field shifted and the anion (broad), high field shifted to negative ppm values. For comparison in our biological studies, the related and known complex $[CpFe(CO)(\kappa^2\text{-dppm})]^+[BF_4]$ (**3**) was also prepared [14d]. Schumann isolated complex **3** in 1987 using a photolytic route starting from a $[CpFe(CO)_2(\kappa^1\text{-dppm})]^+BF_4^-$ which undergoes decarbonylation under UV light affording **3**. We found it convenient to use $[CpFeI(CO)(\kappa^1\text{-dppm})]$ as a precursor which cleanly affords **3** when reacted with NH_4BF_4 or $NaBH_4$ (see SI) as an alternative synthetic route.

Attempts at growing crystals suitable for single crystal X-ray diffraction analysis of compound **4** were exhaustively undertaken, and as with **1a** and **1b** usually resulted, after time periods > 1 week in the deposit of grey/white material and other intractable solids. On one occasion, we noticed the formation of bright yellow needles, which were suitable for single crystal X-ray diffraction analysis, but did not correspond to **4**, rather a decomposition product: $[CpFe(CO)(\kappa^2\text{-dppm})]^+[hfac]^-$ (**4-D**) (Fig. 7), which forms from **4** via formal loss of "$AgI(PMe)_3$". This further underlines the weak bonding interaction between the $hfac^-$ moiety and the $AgI(PMe)_3$, and the anion has a high propensity to lose the Ag containing fragment.

To further elucidate the nature of the elusive anion in **1a, 1b**, and **4**, density functional theory (DFT) calculations were carried out. First, the geometry of the $[AgCl(hfac)(PMe_3)]^-$ was optimised

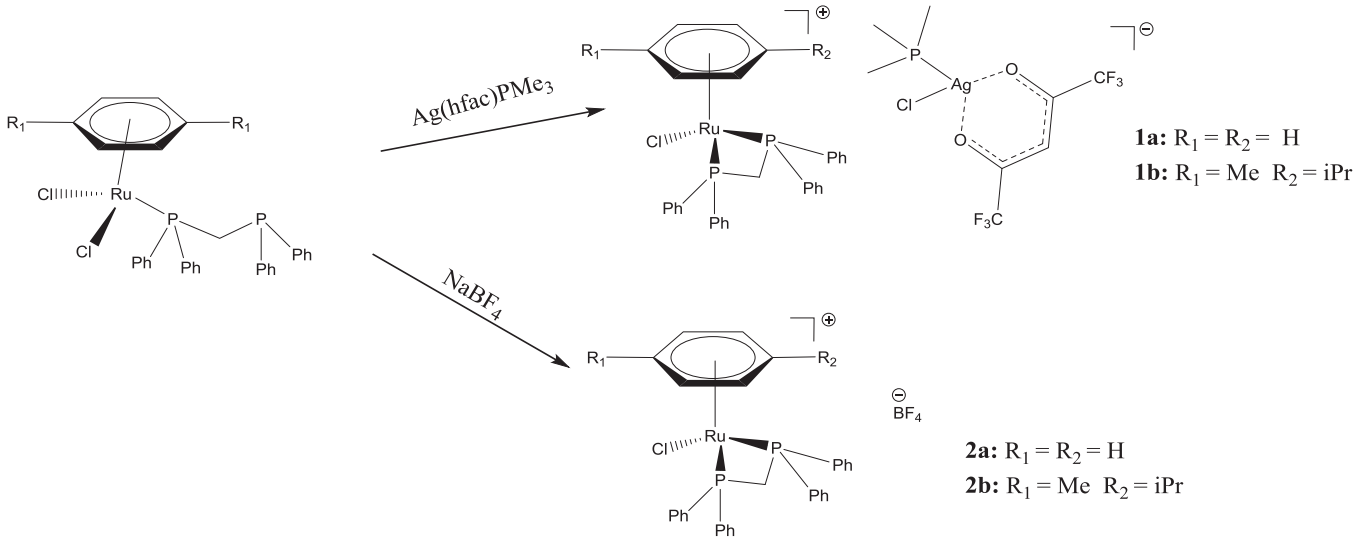

Scheme 1. Reaction scheme for the formation of **1a,b** and **2a,b**. We represent the anion as having a bonding interaction between Ag and O, but this is only a weak interaction (see below).

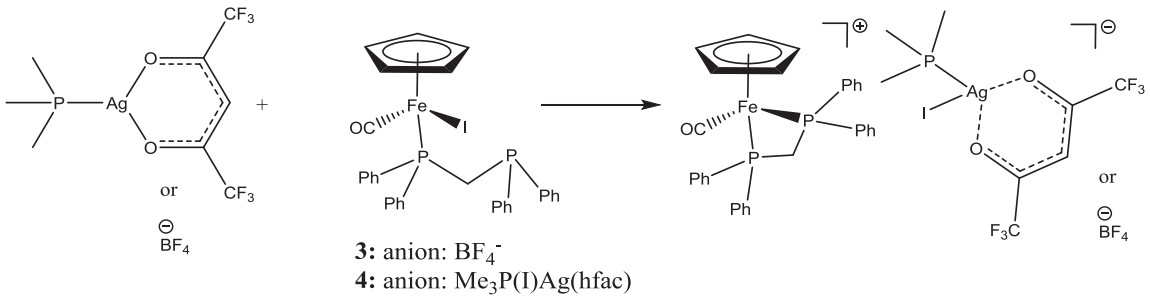

Scheme 2. Reaction scheme of the formation of ionic complexes **3** and **4**.

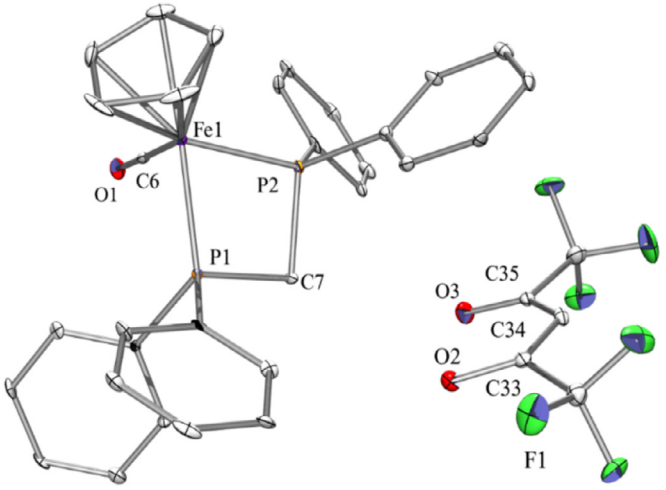

Fig. 7. ORTEP view of **4-D** (cation and anion depicted) clearly showing loss of the "AgI(PMe_3)" moiety from the parent compound **4**. H atoms are omitted for clarity and thermal ellipsoids are at the 30 % level. Bond lengths and angles are available in the supporting information.

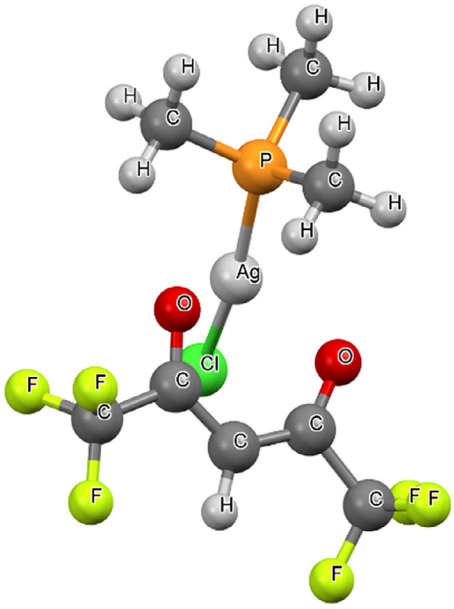

Fig. 8. DFT optimised structure of $[AgCl(hfac)(PMe_3)]^-$ anion. The Cl-Ag-P bond angle is 168.4°.

(see computational details) starting from different starting geometries: tetrahedral and square-planar. The structure with the lowest energy found is presented in Fig. 8.

The Ag-O bond lengths in the optimised structure are 2.75 Å and 3.19 Å, respectively, which shows the interaction between the "$AgCl(PMe_3)$" moiety and the $hfac^-$ is rather weak, in accordance with our experimental observations. Also, the expected linearity of the P-Ag-Cl bond is perturbed by this interaction bending the P-Ag-Cl bond axis to 168.4 °. We also modelled the interaction between $[AgCl(PMe_3)]$ and $hfac^-$ and attempted to find a transition state (TS) via the Nudged Elastic Band method (NEB). While this method could not find a TS, with the energy only lowering along the reaction coordinate, it reveals that the energy of the optimized $[AgCl(hfac)(PMe_3)]^-$ anion is 6.05 kcal/mol lower than the sum of energies of separately optimized $[AgCl(PMe_3)]$ and $(hfac)^-$. This corroborates that $hfac^-$ is bound to "$AgCl(PMe_3)$" moiety, though weakly, being thermodynamically favoured. To further corroborate

Table 1
Experimental vs. calculated IR vibrational frequencies (in cm^{-1}) of C-O in studied complexes. A trend from strongest C-O bond strength in $hfac^-$ to weakest in the complex $[Ag(hfac)PMe_3]$ is clearly seen. The anion $[AgCl(hfac)(PMe_3)]^-$ falls in between these two extremes.

Complex	$hfac^-$	$[AgCl(hfac)(PMe_3)]^-$	$[Ag(hfac)PMe_3]$
$\nu_{sym}^{exp}(CO)$	-	1668 (in **1a**) 1669 (in **1b**)	1648
$\nu_{sym}^{calc}(CO)$	1685	1674	1648

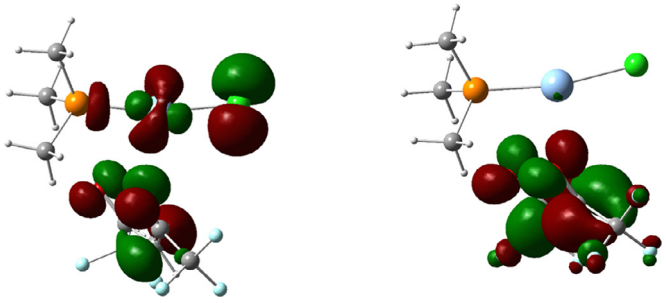

Fig. 9. Computed HOMO (left) and LUMO (right) in $[AgCl(hfac)(PMe_3)]^-$. Orange = phosphorus, blue = silver, grey = oxygen, white = hydrogen, green = chlorine, light blue = fluorine, grey = carbon.

our findings, we compared the calculated infrared spectra of the anion with the experimental IR spectra obtained for complexes **1a** and **1b**. As a reference, we selected the symmetric stretching mode of C=O bond in the $hfac^-$ moiety. There is a reasonable agreement between the calculated and experimental frequency for this stretching vibration (Table 1). This provides further evidence, that the DFT calculated structure is correct and that the $hfac^-$ is indeed weakly bound to "$AgCl(PMe_3)$" moiety. For the sake of completeness, we also optimised the structures of the free $hfac^-$ anion and the stable known complex $[Ag(hfac)PMe_3]$ [14a], the latter featuring a strong bonding interaction between the Ag and two O atoms of the hfac moeity (2.268 and 2.309 Å [14a] vs 2.242 and 2.263 Å (our optimised structure)) and computed their IR spectra. As presented in Table 1, there is a good agreement between the calculated C=O vibrational frequencies (see SI for spectra) and those obtained experimentally. Also, the highest frequency corresponding to the symmetric C=O stretching mode in this series is observed in $hfac^-$ (featuring a classical double bond), intermediate the elusive anion $[AgCl(hfac)(PMe_3)]^-$ and lowest value, $[Ag(hfac)PMe_3]$, where coordination between the Ag and O atoms is the strongest. Given that the C=O bond weakens if coordinated to a metal, the strongest C=O bond is in hfac- and weakest in $[Ag(hfac)PMe_3]$ salt. The observed trend in vibrational frequencies supports the fact that in the anion there is some interaction between $AgCl(PMe_3)$ and $hfac^-$, that is, however, weaker than in $[Ag(hfac)PMe_3]$ and provides insight into the bonding interaction and rather labile nature of the anion observed spectroscopically (NMR and ESI-MS).

Moreover, the HOMO and LUMO of the anion $[AgCl(hfac)(PMe_3)]^-$ was also computed: The HOMO (-2.2099 eV) is delocalised over entire anion (Fig. 9), whilst the LUMO (0.5609 eV) is localised on the $hfac^-$ moiety. The delocalisation of the HOMO over the entire molecule is further evidence for a weak bonding interaction between the $hfac^-$ moiety and the "$Ag(PMe_3)Cl$" entity.

3. In vitro studies and short and long- term cytotoxicity and scratch motility assay

The anticancer effects of the ruthenium and iron silver salt compounds were investigated against MCF-7 (ER+), and MDA-

Table 2
IC_{50} values and selectivity indices (SI) of the tested compounds and cisplatin in oestrogen receptor positive (MCF-7) and triple negative (MDA-MB-231) breast cancer cell lines along with normal breast epithelial (MCF-12A).

Compound	Cell Lines				
	MCF-7		MBA-MB-231		MCF-12A
	IC_{50}	SI	IC_{50}	SI	IC_{50}
1a	2.06	4.75	2.25	4.35	9.8
1b	2.47	3.03	1.78	4.21	7.05
2a	2.30	3.15	3.01	2.41	7.26
2b	1.67	5.09	3.70	2.3	8.50
3	1.60	5.73	2.88	3.18	9.17
4	0.83	**9.51**	3.12	2.53	7.90
Cisplatin	5.74	2.26	13.98	0.93	6.87

MB-231 (TNBC) breast cancer cells. To this end, the 3-(4,5 dimethylthiazol-2-yl)-2,5-diphenyltrazolium bromide (MTT) assay was performed and cisplatin was included as a positive control. In addition, to determine the selectivity of the compounds for the breast cancer cells, the normal breast epithelial cells (MCF-12A) were included in these experiments. Figure S36 (See SI) and Table 2 indicate that all the compounds tested, inhibit breast cancer cell viability at concentrations much lower than cisplatin: in MCF-7 cells the IC_{50} values ranged from 0.83 μM (compound **4**) to 2.47 μM (compound **1b**) compared to 5.74 μM for cisplatin and in MDA-MB-231 cells the IC_{50} values ranged from 1.78 μM (compound **1b**) to 3.7 μM (compound **2b**) compared to 13.98 μM for cisplatin. Furthermore, when compared to non-malignant breast epithelial cells (MCF-12A), all complexes exhibit promising selectivity indices (SI) >2.3 which suggest that they are more selective for the breast cancer cells tested. Compounds **1a** and **4** were chosen for further investigation as they exhibited highest selectivity for MDA-MB-231 (**1a**) (4.35) and MCF-7 (**4**) (9.51) cells respectively. Cisplatin showed no selectivity for MDA-MB-231(SI-0.93) cells. It is important to point out that the complexes bearing the silver anion generally outperform their BF_4 counterparts both in terms of activity and selectivity on both cell lines (with some exceptions) pointing to the fact that the anion is involved in cytotoxic action, rather than being a benign counteranion. This is particularly the case comparing complex **3** with **4**, where the latter silver containing compound exhibits much higher cytotoxic activity towards MCF-7 (roughly twice as active) compared to **3**. Also, **4** has a much higher selectivity index on this cell-line than **3** (nearly by a factor 2). Complexes **3** and **4** however perform comparably on the MBA-MB-231 cell line. In addition, comparison of complex **1a** to its BF_4 counterpart **2a** reveals much higher selectivity on both cell lines for **1a**, while comparing **1b** and **2b** shows higher activity and selectivity on MBA-MB-231. Overall, these results support the fact that the silver containing salts perform better overall compared to their BF_4 analogues. The exact mechanism of action of these agents is currently under investigation – but presumably the labile nature of the $[AgX(PMe_3)(hfac)]^-$ anion (see above) likely results in the liberation of $AgX(PMe_3)$ under biological conditions *in vitro* which exerts anti-cancer activity alongside the respective Ru or Fe containing cations, which are cytotoxically active on their own as shown by the salts containing the benign BF_4 anion in this study.

To determine the ability of compounds **4** and **1a** to inhibit long-term survival of MCF-7 and MDA-MB-231 breast cancer cells respectively, clonogenic assays were performed. Fig. 10 shows that compounds **4** and **1a** were indeed able to inhibit the colony forming ability of the MCF-7 and MDA-MB-231 breast cancer lines respectively in a dose dependant manner. Metastasis, a multistep process characterised by migration and invasion of cancer cells, is the most common cause of mortality among cancer patients. We therefore investigated the ability of compounds **4** and **1a** to inhibit the migration of MCF-7 and MDA-MB-231 cells respectively using the scratch motility assay technique. Fig. 11 shows that both the compounds significantly reduced the migratory ability of the breast cancer cell lines tested in a dose dependent manner.

4. Compound 4 and 1a Induces Apoptosis in Breast Cancer Cells

Compounds **4** and **1a** also induced morphological and molecular characteristics of apoptosis in MCF-7 and MDA-MB-231 breast cancer cells respectively (Fig 12). Indeed, they induced cell shrinkage, membrane blebbing and chromatin condensation (Fig 12 A & B) and increased levels of cleaved PARP (Fig 12 C & D).

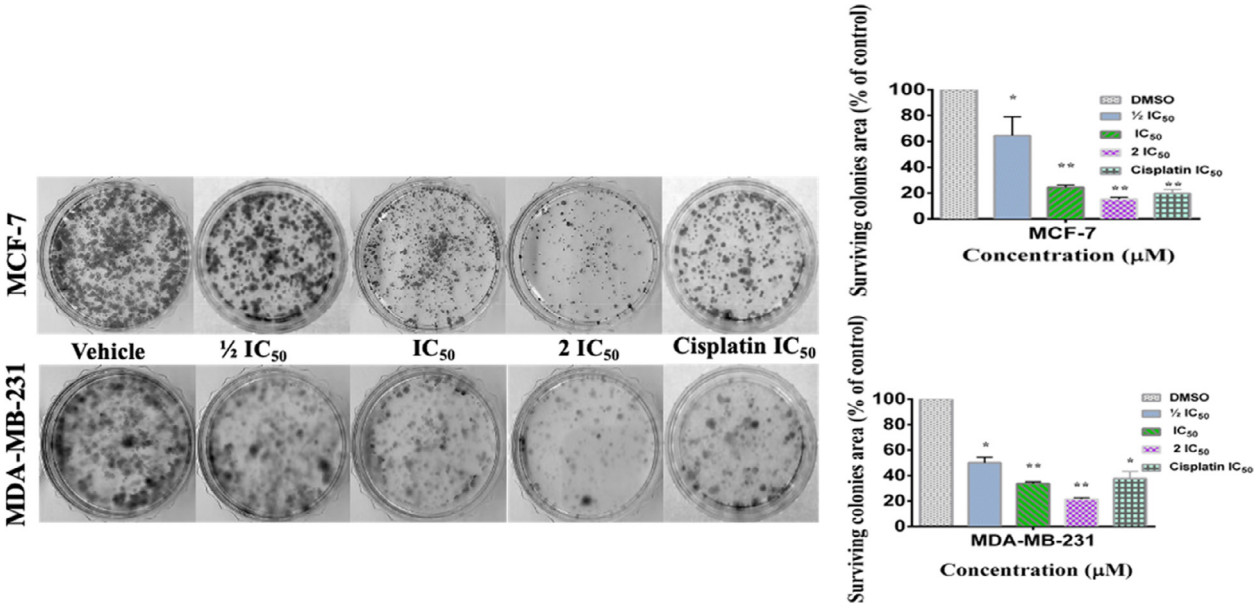

Fig. 10. Compounds **4** and **1a** inhibit the long-term survival of MCF-7 and MDA-MB-231 breast cancer cells. Clonogenic assays were carried out in which each breast cancer cell line was treated with the vehicle or ½ IC_{50}, IC_{50} and 2 IC_{50} of compounds 4 or 1a and IC_{50} cisplatin for 24 h after which the cells were re-plated at low densities (500 cells for MCF-7 and 300 for MDA-MB-231) in drug-free medium and allowed to grow and form colonies up to 14 days. The graph represents the mean colony area ± SEM of each treatment as a percentage of the vehicle control for experiments done in triplicate. Data were analysed using GraphPad Prism 6.0 and a parametric unpaired t-test was performed $^{*}p<0.05$, $^{**}p<0.01$, $^{***}p<0.001$.

5. Conclusion

A series of ruthenium and iron salt complexes have been prepared bearing the elusive anion $[AgX(hfac)(PMe_3)]^-$ and compared to their BF_4^- analogues in terms of anticancer activity. All complexes exhibit considerable anticancer potential towards both breast cancer cell lines tested (MCF-7) and (MDA-MB-231) *in vitro* with selectivity indices (SI) significantly better than cisplatin which was included as a positive control. In general, the presence of silver in the anion boosts cytotoxic activity and selectivity compared to the BF_4 analogues revealing a potential synergic benefit to the incorporation of silver into the salt compounds. Strikingly, the best performing complex in the series is the iron salt complex bearing a silver anion, **4**. Clonogenic assays and scratch mobility assays performed with compounds **1a** and **4**, the two best performing salts from the *in vitro* screening studies, show long term stability of the drugs in a dose dependent manner and inhibition of cell migration. In addition, the results obtained from light microscopic images and western blotting confirm that compounds **1a** and **4** induces apoptotic cell death in MDA-MB-231 and MCF-7 cells respectively. Together, these results suggest that this new class of anticancer agents are highly promising and should be taken forward for pre-clinical studies, in particular complex **4**, which based on iron is a relatively inexpensive metal and performs superior to all the ruthenium complexes tested in this series. The exact biological mechanism of action of the silver containing compounds is currently under exploration in our laboratory, but presumably based on the labile nature of the anion involves expulsion of the $AgCl(PMe_3)$ moiety which acts in accord with the Ru or Fe cation, achieving overall better activities and selectivities. The fate of the $AgCl(PMe_3)$ moiety is under exploration and further mechanistic studies are underway in our laboratory at this time.

6. Experimental section

6.1. General considerations

All reactions were carried out using standard Schlenk and glove-box techniques, but the work-up of the complexes was performed under atmospheric conditions. 1,1-Bis(diphenylphosphino)methane (97%, *dppm*) were purchased from Sigma-Aldrich. (Benzene)ruthenium dichloride(II) dimer (98%), (cymene)ruthenium dichloride(II) dimer (98%), and trimethylphosphane(hexafluoroacetylacetonato)silver(I) (99%, *Ag(hfac)PMe$_3$*) were purchased from Strem Chemicals, Inc. Iodine was purchased from VWR chemicals. Dichloromethane (stab. Amylene), *n*-hexane, acetonitrile, diethyl ether (stab. BHT) and methanol absolute were purchased from Biosolve. Prior to use all solvents were passed through a column of alumina and saturated with nitrogen for 30 minutes. IR-spectra were recorded at room temperature on a MIRacle 10 Shimadzu FTIR spectrometer with an optical range from 5000 cm^{-1} to 650 cm^{-1}. Melting points were determined on a Stuart SMP10 within a range between 0 and 300°C and are uncorrected. The NMR spectra of all compounds were recorded at room temperature on a Bruker NMR machine 300 MHz Ultrashield magnet system in $CDCl_3$ containing TMS as an internal standard. High resolution Electron Ionisation Spray (ESI) mass spectra were recorded using an Orbitrap LTQ XL of Thermo Scientific mass spectrometer at the Technische Universitaet Berlin. In all cases only the relevant signals are noted although there was fragmentation (see SI for the actual spectra). Single crystal X-ray crystallography was performed at a Bruker Smart APEX at the Technische Universität Graz. The synthesis of known compounds **2b** and **3**, the latter being prepared via a different route to literature [14d] are found in the supporting information and $[RuCl_2(\eta^6\text{-arene})(\kappa^1\text{-dppm})]$ (arene = benzene and *p*-cymene) we prepared from literature [13].

6.2. Synthesis of $[RuCl(\eta^6\text{-benzene})(\kappa^2\text{-dppm})]^+$ $[AgCl(hfac)PMe_3]^-$ (*1a*)

100 mg (0.158 mmol,1 eq.) of $[RuCl_2(\eta^6\text{-benzene})(\kappa^1\text{-dppm})]$ was stirred with 62 mg (0.158 mmol, 1 eq.) Ag(hfac)PMe_3 in 20 mL of dichloromethane at room temperature. After 2 hours the solution was evaporated to dryness. After washing with *n*-hexane (3 × 5 mL), a brown solid was isolated and shown to contain a co-crystallised CH_2Cl_2 moiety (222 mg, 0.0216 mmol, quantitative yield). Melting point: 86°C. ^{1}H NMR ($CDCl_3$, 298 K, ppm): δ 7.66 (m, 4H, C^4-*H*, dppm), 7.48 (m, 8H, $C^{2,6\text{ or }3,5}$-*H*, dppm), 7.39 (m, 8H, $C^{2,6\text{ or }3,5}$-*H*, dppm), 6.32 (s, 6H, η^6-C_6H_6), 5.62 (s, 1H, hfac-C*H*), 4.75 (dt, 1H, $^2J_{HaHb}$ = 14.9 Hz $^2J_{HP}$ = 10.2 Hz, P-C$H_{a\ or\ b}$-P), 4.46 (dt, 1H, $^2J_{HaHb}$ = 14.5 Hz $^2J_{HP}$ = 13.2 Hz, P-C$H_{a\ or\ b}$-P), 1.42 (br d, 9H, $^2J_{HP}$ = 8.0 Hz, PCH_3). ^{13}C {^{1}H} NMR ($CDCl_3$, 298 K, ppm): δ 173.4 (q, $^2J_{CF}$ = 29.7 Hz, *C*-CF_3), 132.3-128.3 (*Ph*-dppm), 118.4 (q, $^1J_{CF}$ = 293.1 Hz, CF_3), 93.1 (t, $^2J_{CP}$ = 2.7 Hz, η^6-C_6H_6), 84.4 (br s, hfac-*C*H), 41.1 (br s, P-CH_2-P), 15.3 (d, $^1J_{CP}$ = 21.3 Hz, P(CH_3)$_3$). ^{31}P {^{1}H} NMR ($CDCl_3$, 298 K, ppm): δ 2.5 (s, *P*-CH_2-*P*), -36.4 (br s, *P*(CH_3)$_3$). ^{19}F {^{1}H} NMR ($CDCl_3$, 298 K, ppm): δ -76.4 (s, CF_3). FTIR (cm^{-1}): υ 3058 (vw), 2974 (vw), 2907 (vw), 1668 (m), 1554 (m),

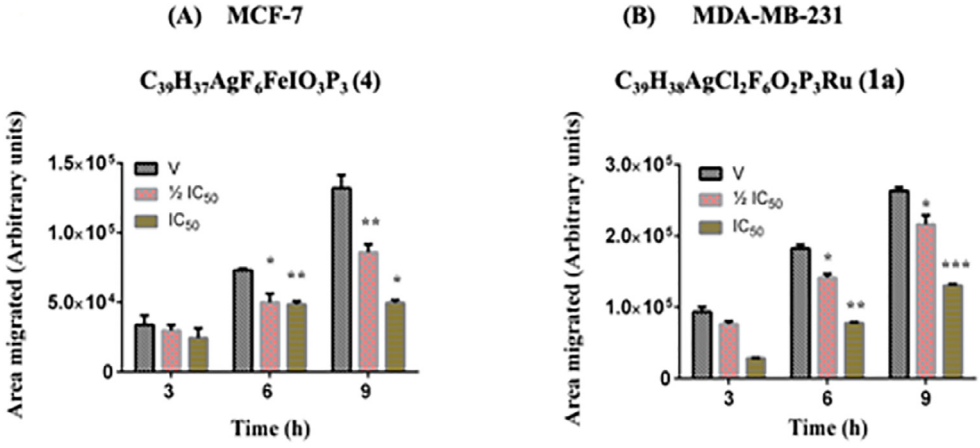

Fig. 11. Compounds **4** and **1a** inhibit migration of breast cancer cells. Plots A and B shows the quantification of scratch motility assays of MCF-7 and MDA-MB-231 breast cancer cells pre-treated with ½ IC_{50} and IC_{50} compounds **1a** and **4** respectively or vehicle for 9 h. Cells were photographed at 0, 3, 6, and 9 h post wound formation. Total area migrated was calculated by subtracting the wound area at each timepoint from the wound area at time 0 which is represented in the graphs as mean area migrated ± SEM pooled from three independent repeats. Data were analysed using GraphPad Prism 6.0 and a parametric unpaired t-test was performed $^*p<0.05$, $^{**}p<0.01$, $^{***}p<0.001$.

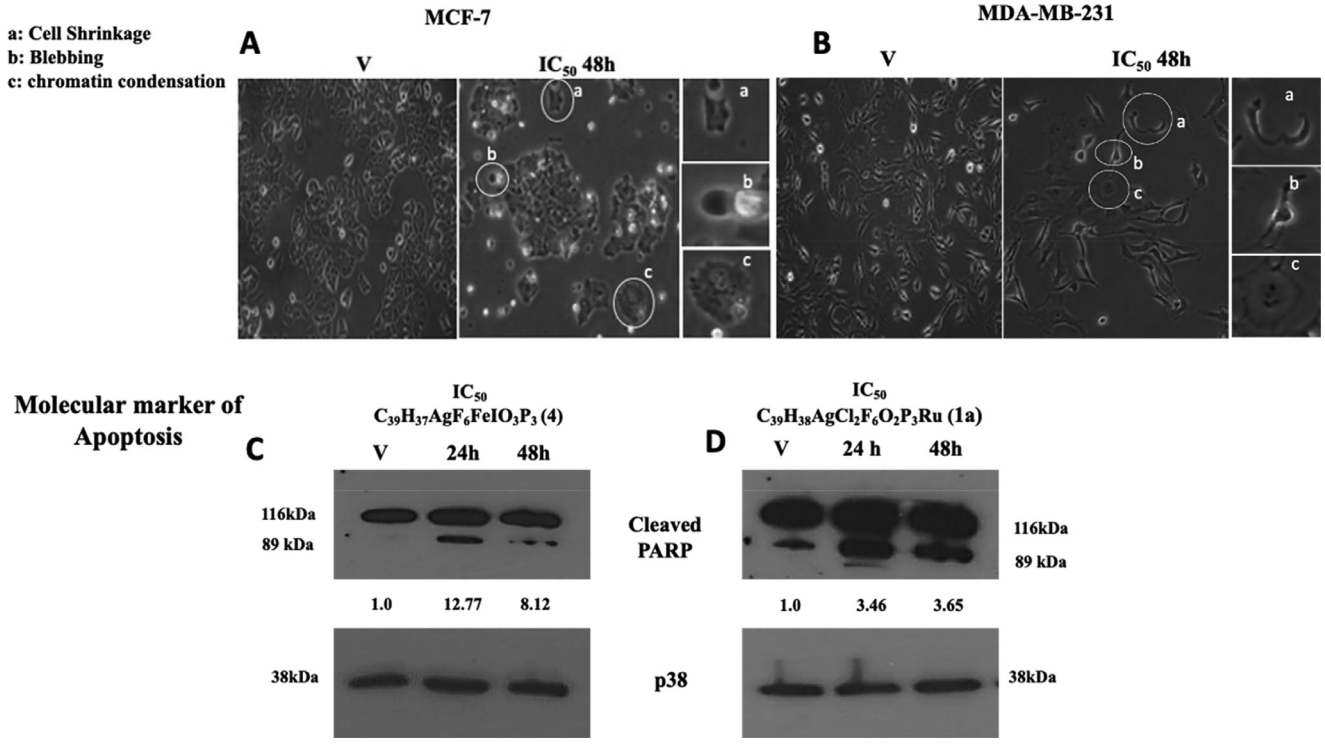

Fig. 12. Compounds **4** and **1a** induces apoptosis in MCF-7 and MDA-MB-231 breast cancer cells respectively. (A) Representative light microcopy images (200x) of cells treated as indicated. Designated circles correspond to magnified images which highlight (a) cell shrinkage, (b) chromatin condensation and (c) membrane blebbing. (B) Western blot analyses of protein harvested from breast cancer cells treated with compounds **4** and **1a** and incubated with antibodies to cleaved PARP. Densitometry readings were obtained using ImageJ and protein expression levels are represented as a ratio of cleaved PARP /p38 normalized to the vehicle control sample.

1528 (m), 1484 (w), 1436 (m), 1309 (vw), 1246 (m), 1178 (s), 1143 (s), 1121 (s), 1100 (s), 1026 (w), 999 (w), 952 (m), 935 (w), 816 (w), 783 (m), 730 (s), 716 (m), 691 (s), 658 (s), 628 (w), 615 (vw), 610 (w). ESI-MS (+) (m/z): calcd. for $[C_{31}H_{28}ClP_2Ru]^+$: 599.0398. Found: 599.0389. ESI-MS (-) (m/z) calcd. for $[hfac]^-$: 206.9881. Found: 206.9885.

6.3. Synthesis of $[RuCl(\eta^6\text{-p-cymene})(\kappa^2\text{-dppm})]^+$ $[AgCl(hfac)PMe_3]^-$ (**1b**)

Compound **1b** was synthesised in analogous fashion as **1a**, in which 177 mg (0.256 mmol, 1eq.) of $[RuCl_2(\eta^6\text{-}p\text{-cymene})(\kappa^1\text{-dppm})]$ and 100 mg (0.256 mmol, 1eq.) of $Ag(hfac)PMe_3$ were dissolved in 10 mL dichloromethane. After 2 hours solvent was evaporated under reduced pressure, which afforded an orange powder (307mg, 0.284 mmol, quantitative yield). ^{1}H NMR ($CDCl_3$, 298 K, ppm): δ 7.66 -7.57 (m, 4H, C^4-*H*, dppm), 7.54 - 7.41 (m, 8H, $C^{2,6\ \&\ 3,5}$-*H*, dppm), 6.27 (br s, 4H, $C^{2,6\ or\ 3,5}$-*H*, η^6-p-cymene), 5.63 (s, 1H, hfac-C*H*), 4.84 (dt, 1H, $^2J_{HaHb}$ = 15.2 Hz, $^2J_{HP}$ = 10.2 Hz, P-C$H_{a\ or\ b}$-P), 4.56 (dt, 1H, $^2J_{HaHb}$ = 15.1 Hz $^2J_{HP}$ = 12.8 Hz, P-C$H_{a\ or\ b}$-P), 2.53 (sept, 1H, $^3J_{HH}$ = 6.9 Hz, C*H*$(CH_3)_2$), 1.53 (s, 3H, CH_3), 1.41 (d, 9H, $^2J_{HP}$ = 8.0 Hz, PCH_3), 1.07 (d, 6H, $^3J_{HH}$ = 6.9 Hz, CH(C$H_3)_2$).^{13}C {^{1}H} NMR ($CDCl_3$, 298 K, ppm): δ 173.2 (q, $^2J_{CF}$ = 29.8 Hz, *C*-CF_3), 132.3-128.6 (*Ph*-dppm), 121.1 (s, $C^{1\ or\ 4}$, η^6-p-cymene), 118.5 (q, $^1J_{CF}$ = 292.3, *C*F_3), 101.5 (s, $C^{1\ or\ 4}$, η^6-p-cymene), 93.3 (t, $^2J_{CP}$ = 3.8 Hz, $C^{2,6\ or\ 3,5}$, η^6-p-cymene), 92.1 (t, $^2J_{CP}$ = 2.1 Hz, $C^{2,6\ or\ 3,5}$, η^6-p-cymene), 84.3 (br s, hfac-*C*H), 42.0 (t, $^1J_{CP}$ = 26.9 Hz, P-*C*H_2-P), 31.0 (s, *C*$(CH_3)_2$), 21.8 (s, C(*C*$H_3)_2$), 17.2 (s, *C*CH_3), 15.3 (d, $^1J_{CP}$ = 21.1 Hz, P(*C*$H_3)_3$).^{31}P {^{1}H} NMR ($CDCl_3$, 298 K, ppm): δ 2.50 (s, *P*-CH_2-*P*), -37.08 (br s, *P*$(CH_3)_3$). ^{19}F{^{1}H} NMR ($CDCl_3$, 298 K, ppm): δ -76.4 (s, *C*F_3). FTIR (cm^{-1}): υ 3056 (vw), 2969 (vw), 2904 (vw), 1685 (w), 1669 (s), 1654 (m), 1647 (w), 1636 (w), 1559 (s), 1540 (m), 1526 (m), 1507 (m), 1482 (w), 1473 (w), 1457 (vw), 1436 (m), 1420 (w), 1309 (vw), 1288 (vw), 1246 (s), 1177 (s), 1145 (s), 1121 (vs), 1098 (s), 1027 (w), 999 (w), 955 (m), 935 (m), 850 (vw), 782 (m), 731 (s), 691 (s), 658 (s). ESI-MS (m/z): calcd. for $[C_{35}H_{36}ClP_2Ru]^+$: 655.1024. Found: 655.1010. ESI-MS (-) (m/z) calcd. for $[hfac]^-$: 206.9881. Found: 206.9893.

6.4. Synthesis of $[RuCl(\eta^6\text{-benzene})(\kappa^2\text{-dppm})]^+BF_4^-$ (**2a**)

18 mg (0.174 mmol, 1.1 eq.) of NH_4BF_4 was added to 100 mg (0.158 mmol, 1 eq.) of $[RuCl_2(\eta^6\text{-benzene})(\kappa^1\text{-dppm})]$ and dissolved in 25 mL of methanol. The solution was heated under reflux at 60°C for 1 hour. The solvent was evaporated under pressure, after which the residue was redissolved in dichloromethane to remove the NH_4Cl through Büchner filtration. After removing the dichloromethane *in vacuo*, a beige powder (102 mg, 0.149 mmol, 94 % yield) was obtained. ^{1}H NMR ($CDCl_3$, 298 K, ppm): δ 7.73–7.64 (m, 4H, C^4-*H*, dppm), 7.53-7.30 (m, 16H, $C^{2,6\ \&3,5}$-*H*, dppm), 6.14 (s, 6H, C_6H_6), 4.87 (dt, 1H, $^2J_{HaHb}$ = 15.0 Hz, $^2J_{HP}$ = 10.6 Hz, P-C$H_{a\ or\ b}$-P), 4.47 (dt, 1H, $^2J_{HaHb}$ = 14.7 Hz $^2J_{HP}$ = 13.3 Hz, P-C$H_{a\ or\ b}$-P). ^{13}C {^{1}H} NMR ($CDCl_3$, 298 K, ppm): δ 132.4 (t, J_{CP} = 5.1 Hz, dppm), 132.1 (br s, dppm), 131.8-131.4 (m, dppm), 129.8 (t, J_{CP} = 5.2 Hz, dppm), 129.0 (t, J_{CP} = 6.1 Hz, dppm), 128.7 (br s, dppm), 128.3 (s, dppm), 93.1 (br s, C_6H_6) 43.3 (m, P-CH_2-P). ^{31}P {^{1}H} NMR ($CDCl_3$, 298 K, ppm): δ 2.06 (s, *P*-CH_2-*P*). ^{19}F {^{1}H} NMR ($CDCl_3$, 298 K, ppm): δ -152.05 (s, BF_4^-). ^{11}B {^{1}H} NMR ($CDCl_3$, 298 K, ppm): δ -0.80 (s, BF_4^-). FTIR (cm^{-1}): υ 3140 (w), 3049 (w), 2916 (w), 2849 (w), 1732 (vw), 1435 (s), 1406 (m), 1188 (vw), 1161 (vw), 1096 (m), 1053 (s), 999 (m), 816 (w), 729 (s), 691 (s). ESI-MS (m/z): calcd. For $[C_{31}H_{28}ClP_2Ru]^+$: 599.0398. Found: 599.0925.

6.5. Synthesis of $[(\eta^5\text{-}C_5H_5)Fe(CO)(\kappa^2\text{-dppm})]^+[AgI(hfac)(PMe_3)]^-$ (4)

320.4 mg (0.485 mmol) of $[CpFe(CO)(\kappa^1\text{-dppm})I]$ and 195.0 mg (0.498 mmol) of $[Ag(PMe_3)(hfac)]$ was dissolved in 10 mL of dried dichloromethane, and stirred at room temperature for 2 hours and

30 minutes. The solvent was removed under reduced pressure and washed with dried n-hexane (3 × 2 mL). The washings were decanted and discarded, and the solid was dried *in vacuo* at room temperature to give an air stable solid of olive brown colour as a hexane solvate. (451.9 mg, 0.430 mmol,. 88.7% yield). Melting point: 69°C + dec. ^{1}H NMR ($CDCl_3$, 298.2 K): δ 7.46 (10H, s, C-*H*, dppm), 7.32 - 7.14 (10H, s, C-*H*, dppm), 5.59 (1H, s, C-*H*, hfac), 4.74 (br m, 1H, PC*H*HP), 4.48 (5H, br s, η^5-C_5H_5), 3.61 (br m, 1H, PCH*H*P), 1.31 (9H, br s, P(CH_3)$_3$), 1.80 (m, hexane) 0.89 (m, hexane). ^{19}F {^{1}H} NMR ($CDCl_3$, 298.2 K): δ -76.4 (s, CF_3). ^{13}C {^{1}H} NMR ($CDCl_3$, 298.2 K): δ 215.6 (br s, Fe*C*O), 173.2 (d, $^{2}J_{CF}$ = 29.7 Hz, *C*-CF_3), 133.7 (s, dppm), 132.5 (s, dppm), 132.2 (d, $^{2}J_{CP}$ = 7.6 Hz, dppm), 131.9 (s, dppm), 131.6 (m, dppm), 130.9 (t, $^{2}J_{CP}$ = 4.9 Hz, dppm), 130.4 (s, dppm), 130.2 (s, dppm), 129.4 (dt, dppm), 128.8 - 128.4 (m, dppm), 118.3 (q, $^{1}J_{CF}$= 290 Hz, *C*F_3), 84.2 (s, hfac-*C*-H), 82.5 (s, η^5-C_5H_5), 43.7 (m, PCH_2P), 31.6 (s, hexane), 22.7 (s, hexane), 15.2 (d, $^{2}J_{CP}$ = 15.3 Hz, P(CH_3)$_2$), 14.4 (s, hexane). ^{31}P {^{1}H} NMR ($CDCl_3$, 298.2 K): δ 26.3 (br s, κ^2-dppm), -44.9 (v br s, $\Delta\nu_{½}$ = 89 Hz, Ag-PMe_3). FTIR: 3674 (vw), 2967 (w), 2901 (w), 2359 (w), 1964 (br s, C≡O stretching), 1670 (s), 1553 (s), 1526 (s), 1483 (w), 1435 (s), 1308 (w), 1244 (s), 1177 (br s), 1144 (br s), 1121 (br, vs), 1098 (br s), 1026 (w), 999 (w), 951 (br s), 845 (w), 783 (w), 731 (s), 691 (s), 658 (s), 584 (w), 552 (w). UV-Vis: (nm)/dichloromethane λ_{max} = 386.0. ESI-MS(+) m/z Calcd. For [M^+] 533.0886. Found 533.0865. ESI-MS(-), m/z Calcd. For [hfac]$^-$ 206.9881. Found 206.9893. Upon prolonged standing in toluene at -25°C, yellow crystals were obtained, which were isolated from decomposed material yielding [(η^5-C_5H_5)Fe(CO)(κ^2-dppm)]$^+$[hfac]$^-$ on the basis of X-ray diffraction analysis. NMR analysis on the crystals: ^{1}H NMR ($CDCl_3$, 298.2 K): δ 7.49 - 7.35 (16H, m, C-*H*, dppm), 7.12 - 7.09 (4H, s, C-*H*, dppm), 5.52 (1H, s, C-*H*, hfac), 5.31 (1H, br, PCH_2P), 4.72 (5H, s, η^5-C_5H_5), 3.86 (1H, br PCH_2P). ^{19}F {^{1}H} NMR ($CDCl_3$, 298.2 K): δ -76.3 (s, CF_3). ^{31}P {^{1}H} NMR ($CDCl_3$, 298.2 K): δ 26.5 (s, κ^2-dppm)

7. Computational details

All density functional theory calculations were carried out with BP86 functional within ORCA 4.2.0 program [15] and are of spin-unrestricted type. TightSCF convergence criterium was used in all computations. The ma-def2-SVP basis set [16] was employed for all atoms. The Resolution of Identity (RI) approximation in combination with auxiliary basis set was employed to speed up the calculations. The auxiliary basis set was created within the AutoAux keyword [17]. The dispersion forces were considered in all calculations by employing the method developed by Stefan Grimme [18] which is implemented in ORCA. All optimised structures were tested for imaginary frequencies to ensure they are true minima. The Cartesian coordinates of optimised structures and the calculated IR spectra are provided in ESI.

8. Cell culture

DMEM (Highveld Biologicals, Lyndhurst, United Kingdom (UK) and RPMI 1640 (Highveld Biologicals, Lyndhurst, United Kingdom (UK) were used to maintain human breast adenocarcinoma cells MDA-MB-231 (triple negative) and MCF-7 (oestrogen receptor positive) respectively. A 1:1 mixture of DMEM and Ham's F 12 (Highveld Biologicals, Lyndhurst, United Kingdom (UK), supplemented with 20 ng/mL of human epidermal growth factor, 100 ng/mL of cholera toxin, 0.01 mg/mL of bovine insulin and 500 ng/mL of hydrocortisone was prepared aseptically for the maintenance of the non-tumourigenic breast epithelial MCF-12A. When treated with the test compounds, the MCF-12A cells were cultured in non-supplemented medium. Cells were maintained at 37 °C in a 5% CO_2– 95% air-humidified incubator [19, 20].

9. Cell treatments

The compounds **1a, 1b, 2a, 2b, 3** and **4** were dissolved in dimethyl sulfoxide (DMSO) (Merck 48856212719) to achieve a final stock concentration of 5 mM and heated at 100° C for 2 min and stored at room temperature for a maximum of 5 days before use. The 5 mM stock solutions were further diluted using cell culture medium to attain final experimental concentrations (2, 4, 6, 8 and 10 μM) and a vehicle control (DMSO) of equivalent highest compound concentration was prepared simultaneously. Cisplatin was used as the positive control at its reported IC_{50} values for MCF-7, MDA-MB-231 and MCF-12A cells [19, 20].

10. Cytotoxicity assay

The MCF-7 and MDA-MB-231 breast cancer cells along with MCF-12A normal breast epithelial cells were plated in 96-well plates and treated with a range of concentrations (2, 4, 6, 8 and 10 µM) of the compounds or vehicle (DMSO) at a concentration of 10 µM for a period of 48 h. Cytotoxicity of these compounds were evaluated using the 3-(4,5 dimethylthiazol-2-yl)-2,5-diphenyltrazolium bromide (MTT) assay (M21281G, Sigma-Aldrich) according to the manufacturer's instructions. The mean cell viability was calculated as a percentage of the mean of the vehicle control. At least three independent experiments in quadruplicate were performed from which the half maximal inhibitory concentration (IC_{50}) was determined using graph prism version 6.0. The selectivity index (SI) was calculated using the following formula (IC_{50} of normal breast epithelial cells) / (IC_{50} of tumourigenic cell line) [19, 20, 23].

11. Clonogenic assay

MCF-7 and MDA-MB-231 cells were seeded in 6-well plates and treated with ½ IC_{50}, IC_{50}, 2 IC_{50} of compounds **1a** and **4** respectively and vehicle. After 24 h, 500 cells for MCF-7 and 300 for MDA-MB-231 were seeded in 35 mm dishes in drug free medium. The formation of colonies was monitored and after 14 days the surviving cells were fixed and stained with crystal violet (Sigma-Aldrich, USA). Colonies were imaged and percentage colony area was determined using Image J v 1.50i software. Colony area was determined for each concentration of compound and expressed as a percentage of vehicle-treated control [19, 20, 23].

12. Scratch motility assay

MCF-7 and MDA-MB-231 cells were seeded in 6-well plates and was incubated for 24 and 48 h respectively to obtain a 100% confluent monolayer of cells. Following the incubation period prior to the treatment a vertical scratch was made with the help of a 2 μL pipette tip in the cell monolayer of each well. The cells were treated with vehicle and ½ IC_{50}, IC_{50} concentrations of the compounds **1a** (MDA-MB-231) and **4** (MCF-7), respectively. Cells were treated with 10 μL of mitomycin C (M4287; Sigma Aldrich) to inhibit proliferation. Light microscopic images were recorded at 0, 3, 6, and 9 h post wound formation and image J (version 2.0.0-rc-69/1.52p) was used to calculate the area of the scratch. The total areas migrated was determined by subtracting the area for a specific time point from the area measured at 0 h [19, 21, 22].

13. Western blotting

The MCF-7 and MDA-MB-231 breast cancer cells were treated with vehicle and IC_{50} concentrations of compounds 4 and 1a for 24 and 48 h. Following treatment the cells were lysed in whole-cell lysis buffer and western blotting was carried out as previously

described [19]. The primary antibody used in this study was PARP (#9542) from Cell signaling technologies (Massachusetts, USA). Following the primary antibody incubation, membranes were incubated with goat ant-rabbit HRP-conjugated secondary antibodies (Bio-Rd Laboratories, California, USA) and p38 was used as a loading control. Image J software version 2.0.0-rc-69/1.52p was used for obtaining the densitometric readings. The protein expression levels are represented as a ratio of protein of interest/p38 normalized to the vehicle control sample.

14. Statistical analysis

Statistical analysis was conducted with the acquisition of the data represented as mean values and SEM (standard error of the means) of three independent experiments. The t-test (a student's statistical hypothesis test) was used to compare the two experimental frames and a value of $p < 0.5$ was accepted as statistically significant.

Supporting Information: Supplementary information containing all spectral data, X-ray data with bond angles and bond lengths, synthesis of known complexes, and tables of cartesian coordinates with additional information on the DFT calculations is available. The X-ray structure of **4-D** is available at the CSD (Deposition Number 2049254). These data can be obtained free of charge from The Cambridge Crystallographic data Center via the link http://www.ccdc.cam.ac.uk/data_request/cif

Declaration of Competing Interest

The authors declare that they have no known competing financial interests or personal relationships that could have appeared to influence the work reported in this paper.

Acknowledgements

We would like to thank the Maastricht Science Programme (MSP) and Maastricht University (Faculty of Science and Engineering, FSE) for financial support of this research. We thank Dr. Maria Schlangen-Ahl (TU Berlin) for recording HRMS of all complexes and Maarten Honing (UM, FHML) and Yuandi Zhao (UM, FHML) for the ESI-MS of complex **2a**. This work was supported by grants from the South Africa Medical Research Council (SA MRC), the South Africa National Research Foundation (NRF) (CPRR120815), Cancer Association of South Africa (CANSA) and the University of Cape Town (UCT).

Supplementary materials

Supplementary material associated with this article can be found, in the online version, at doi:10.1016/j.jorganchem.2020.121659.

References

[1] (a) G. Gasser, I. Ott, N. Metzler-Nolte, Journal of Medicinal Chemistry 54 (2011) 3–25; b) S. Dasari, P.Bernard Tchounwou, European Journal of Pharmacology 740 (2014) 364–378.
[2] (a) B. Rosenberg, L. Vancamp, T. Krigas, Nature 205 (1965) 698–699; (b) B. Rosenberg, L. Vancamp, J.E. Trosko, V.H. Mansour, Nature 222 (1969) 385–386.
[3] (a) G.A. Curt, J.J. Grygiel, B.J. Corden, R.F. Ozols, R.B. Weiss, D.T. Tell, C.E. Myers, J.M. Collins, Cancer Research 43 (1983) 4470–4473; (b) M. Rozencweig, C. Nicaise, M. Beer, N. Crespeigne, M.V. Rijmenant, L. Lenaz, Y. Kenis, Journal of Clinical Oncology 1 (1983) 621–626; (c) E.A. Eisenhauer, K.D. Swenerton, J.F. Sturgeon, S. Fine, S.E. O'Reilly, Cancer treatment reports 70 (1986) 1195–1198; (d) S. Cowherd, L.D. Miller, S.A. Melin, S. Akman, S. Isom, J. Cole, A. Pullikuth, J.A. Lawrence, Cancer Biology & Therapy 16 (2015) 678–683.
[4] (a) Y. Kidani, K. Inagaki, M. Iigo, A. Hoshi, K. Kuretani, Journal of Medicinal Chemistry 21 (1978) 1315–1318; (b) G. Mathé, Y. Kidani, M. Noji, R. Maral, C. Bourut, E. Chenu, Cancer Letters 27 (1985) 135–143; (c) D. Machover, E. Diaz-Rubio, A. de Gramont, A. Schilf, J.J. Gastiaburu, S. Brienza, M. Itzhaki, G. Metzger, D. N'Daw, J. Vignoud, A. Abad, E. François, E. Gamelin, M. Marty, J. Sastre, J.F. Seitz, M. Ychou, Annals of Oncology 7 (1996) 95–98.
[5] (a) A.E. Taylor, E. Wiltshaw, M.E. Gore, I. Fryatt, C. Fisher, J Clin Oncol 12 (1994) 2066–2070; (b) A. de Gramont, J. Vignoud, C. Tournigand, C. Louvet, T. André, C. Varette, E. Raymond, S. Moreau, N.Le Bail, M. Krulik, European Journal of Cancer 33 (1997) 214–219.
[6] (a) N.J. Wheate, S. Walker, G.E. Craig, R. Oun, Dalton Trans 39 (2010) 8113–8127; (b) M. Galanski, B.K. Keppler, Anticancer Agents Med Chem 7 (2007) 55–73.
[7] (a) J. Fernández-Gallardo, B.T. Elie, F.J. Sulzmaier, M. Sanaú, J.W. Ramos, M. Contel, Organometallics 33 (2014) 6669–6681; (b) J.F. González-Pantoja, M. Stern, A.A. Jarzecki, E. Royo, E. Robles-Escajeda, A. Varela-Ramírez, R.J. Aguilera, M. Contel, Inorganic Chemistry 50 (2011) 11099–11110.
[8] (a) P. Köpf-Maier, H. Köpf, E.W. Neuse, Angewandte Chemie International Edition 23 (1984) 456–457; (b) A.C. Gonçalves, T.S. Morais, M.P. Robalo, F. Marques, F. Avecilla, C.P. Matos, I. Santos, A.I. Tomaz, M.H. Garcia, Journal of Inorganic Biochemistry 129 (2013) 1–8; (c) A. Valente, A.M. Santos, L. Côrte-Real, M.P. Robalo, V. Moreno, M. Font-Bardia, T. Calvet, J. Lorenzo, M.H. Garcia, Journal of Organometallic Chemistry 756 (2014) 52–60; (d) A. Pilon, P. Gírio, G. Nogueira, F. Avecilla, H. Adams, J. Lorenzo, M.H. Garcia, A. Valente, Journal of Organometallic Chemistry 852 (2017) 34–42.
[9] (a) J.M. Rademaker-Lakhai, D. van den Bongard, D. Pluim, J.H. Beijnen, J.H. Schellens, Clinical cancer research: an official journal of the American Association for Cancer Research 10 (2004) 3717–3727; (b) C. Scolaro, A. Bergamo, L. Brescacin, R. Delfino, M. Cocchietto, G. Laurenczy, T.J. Geldbach, G. Sava, P.J. Dyson, Journal of Medicinal Chemistry 48 (2005) 4161–4171; (c) C.G. Hartinger, S. Zorbas-Seifried, M.A. Jakupec, B. Kynast, H. Zorbas, B.K. Keppler, Journal of Inorganic Biochemistry 100 (2006) 891–904; (d) C. Gossens, I. Tavernelli, U. Rothlisberger, Journal of the American Chemical Society 130 (2008) 10921–10928; (e) A. Weiss, R.H. Berndsen, M. Dubois, C. Müller, R. Schibli, A.W. Griffioen, P.J. Dyson, P. Nowak-Sliwinska, Chemical Science 5 (2014) 4742–4748.
[10] (a) V.T. Yilmaz, E. Gocmen, C. Icsel, M. Cengiz, S.Y. Susluer, O. Buyukgungor, Journal of Photochemistry and Photobiology B: Biology 131 (2014) 31–42; (b) Z. Human, A. Munyaneza, B. Omondi, N.M. Sanabria, R. Meijboom, M.J.J.B. Cronjé, BioMetals 28 (2015) 219–228; (c) E. Ferreira, A. Munyaneza, B. Omondi, R. Meijboom, M.J.J.B. Cronjé, BioMetals 28 (2015) 765–781; (d) C. Gibard, K. Fauché, R. Guillot, L. Jouffret, M. Traïkia, A. Gautier, F. Cisnetti, Journal of Organometallic Chemistry 840 (2017) 70–74; (e) Z. Engelbrecht, K. Potgieter, Z. Mpela, R. Malgas-Enus, R. Meijboom, M.J. Cronje, Anti-Cancer Agents in Medicinal Chemistry- Anti-Cancer Agents 18 (2018) 394–400; (f) Z. Engelbrecht, R. Meijboom, M.J.J.B. Cronjé, BioMetals 31 (2018) 189–202.
[11] L. Massai, J. Fernández-Gallardo, A. Guerri, A. Arcangeli, S. Pillozzi, M.a. Contel, L. Messori, Dalton Transactions 44 (2015) 11067–11076.
[12] M. Wenzel, E. Bigaeva, P. Richard, P.Le Gendre, M. Picquet, A. Casini, E. Bodio, Journal of Inorganic Biochemistry 141 (2014) 10–16.
[13] B. Herry, L.K. Batchelor, B. Roufosse, D. Romano, J. Baumgartner, M. Borzova, T. Reifenstahl, T. Collins, A. Benamrane, J. Weggelaar, M.C. Correia, P.J. Dyson, B. Blom, Journal of Organometallic Chemistry 901 (2019) 120934.
[14] (a) N.H. Dryden, J.J. Vittal, R.J. Puddephatt, Chemistry of Materials 5 (1993) 765–766; (b) C. Daguenet, R. Scopelliti, P.J. Dyson, Organometallics 23 (2004) 4849–4857; (c) M. Gaye, C. M'Backe N'Diaye, A. Samb, Bulletin of the Chemical Society of Ethiopia 7 (1993) 117–120; (d) H. Schumann, Journal of Organometallic Chemistry 320 (1987) 145–162.
[15] (a) F. Neese, WIREs Computational Molecular Science 2 (2012) 73–78; (b) F. Neese, WIREs Computational Molecular Science 8 (2018) e1327.
[16] (a) F. Weigend, R. Ahlrichs, Physical Chemistry Chemical Physics 7 (2005) 3297–3305; (b) J. Zheng, X. Xu, D.G. Truhlar, Theoretical Chemistry Accounts 128 (2011) 295–305.
[17] G.L. Stoychev, A.A. Auer, F. Neese, Journal of Chemical Theory and Computation 13 (2017) 554–562.
[18] (a) S. Grimme, S. Ehrlich, L. Goerigk, Journal of Computational Chemistry 32 (2011) 1456–1465; (b) S. Grimme, J. Antony, S. Ehrlich, H. Krieg, The Journal of Chemical Physics 132 (2010) 154104.
[19] J.S. Bleloch, A. du Toit, L. Gibhard, S. Kimani, R.D. Ballim, M. Lee, A. Blanckenberg, S. Mapolie, L. Wiesner, B. Loos, S. Prince, Cell Death Discov (2019) 60.
[20] S. Aliwaini, J. Peres, W.L. Kröger, A. Blanckenberg, J. de la Mare, A.L. Edkins, S. Mapolie, S. Prince, Cancer Letters 357 (2015) 206–218.
[21] L.M. Balsa, M.C. Ruiz, L. Santa Maria de la Parra, E.J. Baran, I.E. León, Journal of Inorganic Biochemistry 204 (2020) 110975.
[22] E. Ortega, A. Zamora, U. Basu, P. Lippmann, V. Rodríguez, C. Janiak, I. Ott, J. Ruiz, Journal of Inorganic Biochemistry 203 (2020) 110910.
[23] N. Aldeghi, D. Romano, C. Marschner, S. Biswas, S. Chakraborty, S. Prince, S. Ngubane, B. Blom, Journal of Organometallic Chemistry 916 (2020) 121214.